JOURNAL OF SOLID STATE CHEMISTRY 115, 240–246 (1995)

Synthesis and Structure of $NaMn_3(PO_4)(HPO_4)_2$, an Unoxidized Variant of the Alluaudite Structure Type

F. Leroux, A. Mar, C. Payen, D. Guyomard, A. Verbaere, and Y. Piffard*

Institut des Matériaux, Laboratoire de Chimie des Solides, UMR 110 CNRS, Université de Nantes, 2, rue de la Houssinière, 44072 Nantes Cedex 03, France

Received April 5, 1994; in revised form July 25, 1994; Accepted July 28, 1994

Sodium manganese(II) phosphate bis(hydrogenphosphate), $NaMn_3(PO_4)(HPO_4)_2$, has been prepared hydrothermally and its structure has been determined from single-crystal diffraction data. It crystallizes in space group $C2/c$ of the monoclinic system with $Z = 4$ in a cell of dimensions $a = 12.179(2)$ Å, $b = 12.405(1)$ Å, $c = 6.6602(8)$ Å, and $\beta = 114.616(7)°$. The structure consists of a complex network of edge-sharing $Mn(II)O_6$ octahedral chains that are linked together by both corner-sharing PO_4 tetrahedra and O–H···O bonds, forming channels along which Na atoms reside. The structure thus represents an *unoxidized* variant of the alluaudite structure type, containing Mn atoms in only the single oxidation state of *+II*. The structure is embellished by the presence of hydrogen bonds, evidence for which was obtained from bond-valence calculations, infrared spectroscopy, and thermal measurements which suggest the loss of one H_2O molecule per formula unit. Magnetic susceptibility measurements confirm the assignment of high-spin Mn^{2+} in the title compound, as well as in its dehydrated form.

INTRODUCTION

The alluaudite structure type is a common one in mineralogy, embracing a wide variety of compounds, largely phosphates, with the general formulation $X(2)X(1)M(1)M(2)_2(PO_4)_3$ (with $Z = 4$), in which $X(2)$ and $X(1)$ are large unipositive or dipositive cation sites (usually filled with Na or Ca, or left vacant) and $M(1)$ and $M(2)$ are invariably occupied by some distribution of Mn^{2+}, Fe^{2+}, or Fe^{3+} (1, 2). Thus, for instance, most natural samples have compositions like (Na, □)(Na, Ca)$(Mn^{2+})(Fe^{2+}, Fe^{3+})_2(PO_4)_3$, where □ is a vacancy (2). Interestingly, however, neither the fully unoxidized nor the fully oxidized members, exemplified by the hypothetical end-member compositions $NaCaMn^{2+}(Fe^{2+})_2(PO_4)_3$ and $Mn^{3+}(Fe^{3+})_2(PO_4)_3$, respectively, have ever been found or prepared. We report here, for the first time to our knowledge, an example of a fully unoxidized end member, $NaH_2Mn^{2+}(Mn^{2+})_2(PO_4)_3$ (alternatively formulated as $NaMn_3(PO_4)(HPO_4)_2$), synthesized under reducing, hydrothermal conditions. We describe its relationship to the alluaudite structure type and report its thermal and magnetic properties.

* To whom correspondence should be addressed.

EXPERIMENTAL

Synthesis. Crystals of $NaMn_3(PO_4)(HPO_4)_2$ were prepared by hydrothermal synthesis. A mixture of $H_2Mn_4O_9 \cdot xH_2O$ (rancieite) (414 mg, 1.0 mmol), H_3PO_4 (10 mmol, 1.0 *M*), NaOH (168 mg, 4.0 mmol), and 1,4-diazabicyclo[2.2.2]octane (DABCO) (219 mg, 2.0 mmol) was placed in a Teflon vessel which was filled to a degree of 80% with water (final pH 2) and enclosed in a stainless steel bomb. The starting material, rancieite, a hydrated phyllomanganate (3), was chosen for its high specific surface area (>300 $m^2 g^{-1}$) and thus its reactivity; its formula was calculated from TGA measurements to obtain the degree of hydration and from redox back titration measurements to obtain the Mn oxidation state. The mixture was heated at 180°C under autogenous pressure for 1 week, affording colorless, needle-shaped crystals of sufficient size for crystallographic study. These crystals contained Na, Mn, and P in an atomic ratio of 1:3:3, as revealed from a microprobe analysis on a scanning electron microscope.

Structure determination. Initial photographic work revealed monoclinic symmetry and gave preliminary cell parameters. The cell parameters were refined from powder diffraction data collected on an INEL multidetector system ($\lambda(CuK\alpha_1) = 1.54056$ Å; Si standard). Table 1 lists observed and calculated interplanar distances as well as the intensities calculated from the crystal structure with the use of the program LAZY-PULVERIX (4). Single-crystal intensity data were collected at room temperature on a Siemens P4 diffractometer under the conditions given in Table 2. Data reduction, structure solution, and refinements were carried out with the use of programs in the SHELXTL PLUS package (5). Analysis of the intensity data revealed the systematic absences (*hkl*, $h + k =$

0022-4596/95 $6.00

TABLE 1
X-Ray Powder Diffraction Pattern of $NaMn_3(PO_4)(HPO_4)_2$

hkl	d_{obs} (Å)	d_{calc} (Å)	I/I_0	*hkl*	d_{obs} (Å)	d_{calc} (Å)	I/I_0
110	8.254	8.260	11	510	2.180	2.180	24
020	6.206	6.202	50	44$\bar{1}$	2.171	2.172	5
200	5.530	5.536	36	31$\bar{3}$	2.163	2.164	33
111	4.290	4.289	12	060	2.067	2.068	3
130	3.873	3.874	21	350	2.059	2.059	13
310	3.537	3.537	45	53$\bar{2}$	2.011	2.011	22
20$\bar{2}$	3.298	3.296	5	602	1.986	1.986	3
11$\bar{2}$	3.180	3.180	94	530	1.953	1.952	4
040	3.101	3.101	18	33$\bar{3}$	1.941	1.941	4
131	3.067	3.066	33	260	1.936	1.937	4
002	3.028	3.027	26	261	1.928	1.928	8
31$\bar{2}$	2.956	2.956	15	600	1.845	1.845	6
22$\bar{2}$	2.910	2.911	4				
400	2.768	2.768	22	511	1.825	1.826	11
041		2.760	28	351		1.824	10
330	2.754	2.753	78	332	1.780	1.780	24
240	2.705	2.706	100	261	1.771	1.771	6
24$\bar{1}$	2.681	2.682	18	170	1.749	1.750	9
40$\bar{2}$	2.671	2.671	42	62$\bar{3}$	1.711	1.711	5
311	2.632	2.631	3	17$\bar{1}$		1.711	2
11$\bar{2}$	2.594	2.594	16	133	1.691	1.692	4
13$\bar{2}$	2.574	2.574	51	043		1.692	7
420	2.528	2.528	25	55$\bar{2}$	1.687	1.687	5
42$\bar{2}$	2.453	2.453	6	64$\bar{2}$	1.672	1.672	20
15$\bar{1}$	2.321	2.322	4	550	1.651	1.652	7
241	2.302	2.302	11	20$\bar{4}$	1.645	1.645	25
20$\bar{2}$	2.286	2.286	7	46$\bar{2}$	1.634	1.635	10
51$\bar{2}$	2.263	2.263	3	15$\bar{3}$	1.624	1.625	12

TABLE 2
Crystal Data and Intensity Collection for $NaMn_3(PO_4)(HPO_4)_2$

Formula	$NaMn_3(PO_4)(HPO_4)_2$
Formula mass (amu)	474.73
Space group	*C2/c*
a (Å)	12.179(2)
b (Å)	12.405(1)
c (Å)	6.6602(8)
β (°)	114.616(7)
V (Å^3)	914.7(2)
Z	4
ρ_c (g cm^{-3})	3.45
μ(Mo*K*α) (cm^{-1})	47.1
Crystal dimensions	0.06 × 0.06 × 0.20 mm
Radiation	Mo*K*α, λ = 0.7107 Å
Scan mode	ω
Scan range (°)	1.2 + $\Delta\theta(\alpha_1, \alpha_2)$
2θ limits (°)	3.0–72.0
Data collected	$\pm h$, $+k$, $+l$
No. of data collected	4656
No. of unique data	2001 (R_{int} = 0.022)
No. of unique data, with $I > 2\sigma(I)$	958
No. of variables	92 (including anisotropic temperature factors)
$R(F)^a$	0.044
$R_w(F)^b$	0.026
GOF	0.93

^{a} $R(F) = \Sigma||F_0| - |F_c||/\Sigma|F_0|$.
^{b} $R_w(F) = [\Sigma w(|F_0| - |F_c|)^2/\Sigma wF_0^2]^{1/2}$, with $w = 1/\sigma^2(F)$.

$2n + 1$; $h0l$, $l = 2n + 1$), consistent with the space groups *C2/c* and *Cc*. The centrosymmetric space group *C2/c* was chosen on the basis of the intensity statistics and the satisfactory refinement of the structure. Conventional atomic scattering factors and anomalous dispersion corrections were used (6). An absorption correction was not deemed necessary. The positions of the Na, Mn, P, and O atoms were determined by direct methods and successive difference Fourier syntheses. The structure was then refined by least-squares methods, involving anisotropic thermal parameters for all atoms. At this stage, a bond-valence sum calculation (7, 8) showed that the Mn atoms were probably all in oxidation state +II (V(Mn(1)) = 1.79 and V(Mn(2)) = 2.12). It became evident that in order to maintain charge balance in the formula, some missing positive charge would have to be found. Two of the oxygen atoms had valence sums that were anomalously low (V(O(2)) = 1.47 and V(O(4)) = 1.27) compared to the expected value of 2. These observations suggested the presence of hydrogen atoms, which were located by inspecting a difference electron density map in the environs of O(2) and O(4). The position of the H atom was refined, and as this converged to yield chemically reasonable O–H···O distances and angles, its isotropic thermal parameter was also refined. Moreover, the introduction of the H atom now brings the bond-valence sums of O(2) and O(4) to more reasonable values of 1.72 and 1.84, respectively (Table 3). The final cycle of refinement on *F* on 958 reflections with $I > 2\sigma(I)$ and 92 variables converged to residuals of $R = 0.044$ and $R_w = 0.026$. The extrema in the final difference electron density map are $(\Delta\rho)_{max} = 0.9$ and $(\Delta\rho)_{min} = -1.0$ e^- Å^{-3}. The final positional and thermal parameters are given in Tables 4 and 5. A list of structure amplitudes is available as supplementary material.

Physical measurements. Infrared spectra were obtained on a 20SCX FTIR spectrometer with the use of KBr pellets. Thermal measurements were made on a

TABLE 3
Bond-Valence Sums for Atoms in $NaMn_3(PO_4)(HPO_4)_2$

Atom	*V*	Atom	*V*
Mn(1)	1.79	O(1)	1.83
Mn(2)	2.12	O(2)	1.72
P(1)	4.68	O(3)	1.96
P(2)	4.74	O(4)	1.84
Na	0.94	O(5)	1.94
H	0.78	O(6)	2.05

TABLE 4
Positional and Equivalent Isotropic Thermal Parameters for $NaMn_3(PO_4)(HPO_4)_2$

Atom	Wyckoff position	x	y	z	U_{eq} (Å^2)[a]
Na	4e	0	0.0203(5)	0.75	0.049(2)
Mn(1)	4e	0	0.2861(1)	0.25	0.0118(5)
Mn(2)	8f	0.28949(8)	0.66110(7)	0.3712(2)	0.0094(3)
P(1)	4e	0	0.6811(2)	0.25	0.0075(7)
P(2)	8f	0.2141(1)	0.8897(1)	0.1121(3)	0.0078(5)
O(1)	8f	0.4630(3)	0.7493(3)	0.5418(6)	0.011(1)
O(2)	8f	0.1051(3)	0.6067(3)	0.2600(6)	0.011(1)
O(3)	8f	0.3480(3)	0.6702(3)	0.1066(6)	0.010(1)
O(4)	8f	0.1496(3)	0.4110(3)	0.3479(6)	0.012(1)
O(5)	8f	0.2137(3)	0.8825(3)	0.3028(6)	0.010(1)
O(6)	8f	0.3482(3)	0.4980(3)	0.4013(6)	0.011(1)
H	8f	0.117(5)	0.491(6)	0.309(11)	0.03(2)[b]

[a] U_{eq} is defined as one-third of the trace of the orthogonalized U_{ij} tensor.
[b] The hydrogen atom was refined isotropically.

Perkin–Elmer TGS-2 thermogravimetric analyzer. Magnetic measurements were conducted on a Quantum Design SQUID magnetometer with the use of powdered samples (~20 mg) that were first cooled to 5 K at zero field and then warmed to 300 K under an applied field of 5 kOe. The data were corrected for contributions from sample holder background and core diamagnetism. Electrochemical experiments with an aim at deintercalation of Na atoms were carried out on a Mac-Pile system under galvanostatic conditions.

RESULTS AND DISCUSSION

Synthesis. As the compound $NaMn_3(PO_4)(HPO_4)_2$ represents a completely unoxidized variant of alluaudite, some details of the synthetic chemistry deserve closer consideration. First, we wish to point out the advantage of the use of rancieite ($H_2Mn_4O_9 \cdot xH_2O$) as a synthetic precursor. It is an already reactive form of manganese oxide (3) (at 470°C it decomposes readily to Mn_2O_3) whose reactivity we hoped would be enhanced even more by the elevated pressures present under hydrothermal conditions. Moreover, the use of rancieite appears to be important for the preparation of phase-pure $NaMn_3(PO_4)(HPO_4)_2$; when MnO_2 is used as the Mn source, for example, the compound is obtained only in minor yield.

As a compound is obtained in which Mn is in the +II oxidation state, it is evident that a reduction of the rancieite took place in the course of the reaction. Thus, it would appear that the protonated DABCO served not as a template as intended, but rather as a reductant having no structural influence on the architecture of the final product. This reducing, acidic environment seems to be why we were able to obtain a synthetic alluaudite analogue in its fully unoxidized form, in contrast to naturally occurring alluaudites, which are invariably found to be partially oxidized and deficient in alkali content.

Description of the structure. Views of the structure of $NaMn_3(PO_4)(HPO_4)_2$ are given in Fig. 1, which shows polyhedral representations of sections of the covalent framework, and Fig. 2, which shows the entire unit cell. The structure of $NaMn_3(PO_4)(HPO_4)_2$ is related to the alluaudite structure type (1), but there are a number of important differences. The covalent framework is built up from a complex arrangement of MnO_6 distorted octahedra and PO_4 tetrahedra. The MnO_6 octahedra share their edges with each other and are grouped into triplets Mn(2)–Mn(1)–Mn(2) to form chains that run along the $[10\bar{1}]$ direction (Fig. 1). These chains are then linked together by PO_4 tetrahedra to form what have been de-

TABLE 5
Anisotropic Thermal Parameters[a] (Å^2) in $NaMn_3(PO_4)(HPO_4)_2$

Atom	U_{11}	U_{22}	U_{33}	U_{12}	U_{13}	U_{23}
Na	0.019(2)	0.110(4)	0.015(2)	0	0.005(2)	0
Mn(1)	0.0123(6)	0.0112(6)	0.0128(7)	0	0.0060(6)	0
Mn(2)	0.0107(4)	0.0080(4)	0.0107(5)	0.0002(4)	0.0056(4)	0.0000(4)
P(1)	0.0071(9)	0.007(1)	0.007(1)	0	0.0019(8)	0
P(2)	0.0099(7)	0.0063(6)	0.0071(8)	−0.0008(6)	0.0034(6)	−0.0001(6)
O(1)	0.010(2)	0.012(2)	0.010(2)	0.001(2)	0.005(2)	−0.002(2)
O(2)	0.007(2)	0.010(2)	0.013(2)	0.000(2)	0.001(2)	−0.004(2)
O(3)	0.012(2)	0.011(2)	0.008(2)	−0.002(2)	0.005(2)	−0.002(2)
O(4)	0.011(2)	0.008(2)	0.016(2)	0.000(2)	0.005(2)	−0.003(2)
O(5)	0.008(2)	0.012(2)	0.009(2)	0.000(2)	0.004(1)	−0.001(2)
O(6)	0.010(2)	0.008(2)	0.014(2)	0.000(1)	0.005(2)	0.002(2)

[a] The form of the anisotropic thermal parameter is $\exp[-2\pi^2(h^2a^{*2}U_{11} + k^2b^{*2}U_{22} + l^2c^{*2}U_{33} + 2hka^*b^*U_{12} + 2hla^*c^*U_{13} + 2klb^*c^*U_{23})]$.

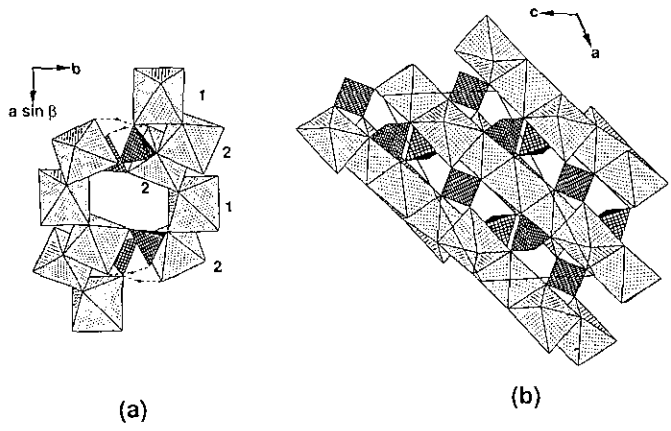

FIG. 1. Views of sections of the covalent framework of $NaMn_3(PO_4)(HPO_4)_2$ as polyhedral representations. The MnO_6 octahedra are dotted and the PO_4 tetrahedra are hatched. (a) Viewed roughly along c, two chains of edge-sharing MnO_6 octahedra, ordered into triplets Mn(2)–Mn(1)–Mn(2), are aligned along the [101] direction (i.e., sloping away from the viewer from top to bottom). (b) Viewed along b, the Mn chains are linked by $P(1)O_4$ and $P(2)O_4$ tetrahedra to form sheets lying parallel to (010). The sheets are joined together in (a) by $P(2)O_4$ tetrahedra and O–H···O bonds.

scribed as "pleated sheets" (1) lying parallel to the (010) plane (Fig. 1b). Within these sheets the $P(1)O_4$ tetrahedra share all four of their vertices with the MnO_6 octahedra: two vertices with one chain and two with an adjacent chain. The $P(2)O_4$ tetrahedra share two of their vertices with one chain and one vertex with an adjacent chain; the fourth vertex points outward away from the plane of the pleated sheet. In turn, the sheets are linked together through this remaining vertex of the $P(2)O_4$ tetrahedra, as well as by hydrogen bonds (Fig. 1a), to form the three-dimensional framework. This framework defines large tunnels in the structure running along the c direction. One tunnel, along 0, 0, z, accommodates Na cations, while the other tunnel, along 0, 1/2, z, is straddled by pairs of O–H···O bonds.

Table 6 lists bond distances and angles around various coordination environments in $NaMn_3(PO_4)(HPO_4)_2$. The average Mn–O distances (Mn(1)–O, 2.236(5); Mn(2)–O, 2.174(5) Å) are more consistent with those in $NaMnPO_4$, in which Mn^{2+} appears (2.230(4) Å) (9), than in $KMn_2O(PO_4)(HPO_4)$, in which Mn^{3+} appears (2.030(1) Å) (10); moreover, they agree well with the sum (2.2 Å) of the ionic radii of Mn^{2+} (0.83 Å) and O^{2-} (1.4 Å) (11). The MnO_6 octahedra appear to be highly distorted, especially around Mn(1), in which the angle subtended by two of the axial oxygens is 156.3(2)°. This distortion probably occurs as a result of the need to accommodate to the connectivity of the PO_4 tetrahedra, which are rather rigid entities and are responsible for holding adjacent chains together. The average P–O distances (P(1)–O, 1.544(5) Å; P(2)–O, 1.541(5) Å) are consistent with those typically observed in phosphates. The $P(2)O_4$ tetrahedron can be considered to be part of an HPO_4 unit, the P(2)–O(4) bond being somewhat weakened (1.590(4) vs 1.524(5) Å (average) for the other three P–O bonds) owing to the presence of the O(4)–H bond.

Two distinct features of the structure of $NaMn_3(PO_4)(HPO_4)_2$ distinguish it from that of the parent alluaudite: the presence of H bonding and the coordination of the Na atom. In terms of the general formulation $X(2)X(1)M(1)M(2)_2(PO_4)_3$ of the parent alluaudite, the $X(1)$ site at 1/2, 0, 0 (and 0, 1/2, 0) resides in a large, distorted cubic coordination environment, while the $X(2)$ site at 0, 0, 0 (and 1/2, 1/2, 0) resides in an irregular rhombic environment (1, 2). Although neither of these sites is occupied in $NaMn_3(PO_4)(HPO_4)_2$, we may associate the O–H···O bridges with the *tunnel* where $X(1)$ is located and the Na atom with that of $X(2)$.

Evidence for O–H bonds was found from bond-valence sum calculations derived from the crystal structure (Table 3), infrared spectroscopy, and TGA measurements. Although hydrogen atom positions found from X-ray data are generally highly uncertain, it is noteworthy that the O–H distance (1.06(7) Å) is precisely that which would be expected for the observed O···O distance (2.503(5) Å), based on known correlations of O–H distance with O···O distance (12). The infrared spectrum clearly shows the presence of broad O–H stretching and bending vibrations centered at 2200 and 1380 cm^{-1}, respectively. The O–H stretching frequency is also in good agreement with that predicted for an O···O distance of ~2.5 Å (12). Thermal

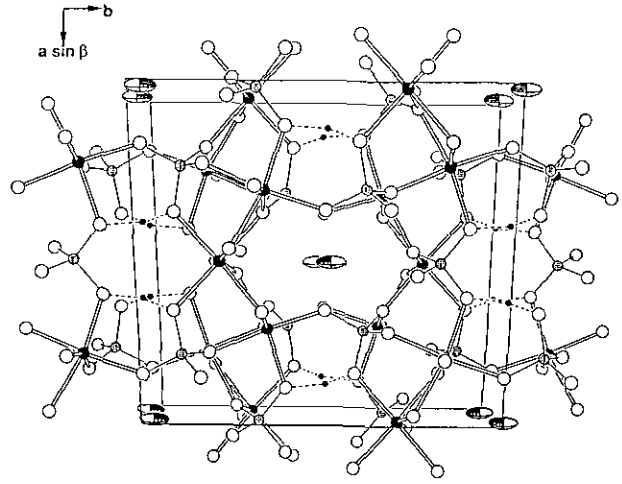

FIG. 2. View of $NaMn_3(PO_4)(HPO_4)_2$ along c, showing the cell outline. The large filled circles are Mn atoms, the shaded circles are P atoms, the open circles are O atoms, the small filled circles are H atoms, and the thermal ellipsoids are Na atoms. There are two kinds of large tunnels, one straddled by O–H···O bonds, and the other occupied by Na atoms.

TABLE 6
Selected Interatomic Distances (Å) and Angles (°) in $NaMn_3(PO_4)(HPO_4)_2$

			$Mn(1)O_6$ octahedron			
Mn(1)	O(1)	O(1)	O(3)	O(3)	O(4)	O(4)
O(1)	2.218(5)	4.340(5)	2.819(5)	3.023(6)	3.647(6)	3.110(5)
O(1)	156.3(2)	2.218(5)	3.023(6)	2.819(5)	3.110(5)	3.647(6)
O(3)	78.8(1)	85.8(1)	2.221(4)	3.387(6)	4.481(5)	3.001(6)
O(3)	85.8(1)	78.8(1)	99.3(2)	2.221(4)	3.001(6)	4.481(5)
O(4)	108.7(1)	87.7(2)	172.1(1)	83.8(1)	2.270(4)	3.320(7)
O(4)	87.7(2)	108.7(1)	83.8(1)	172.1(1)	93.9(2)	2.270(4)
			$Mn(2)O_6$ octahedron			
Mn(2)	O(1)	O(2)	O(3)	O(5)	O(5)	O(6)
O(1)	2.225(4)	4.340(5)	2.819(5)	2.923(5)	2.890(6)	3.385(5)
O(2)	163.6(2)	2.159(4)	3.596(6)	2.947(5)	2.960(5)	3.025(5)
O(3)	79.9(2)	112.7(1)	2.162(5)	3.119(6)	4.302(6)	2.901(6)
O(5)	83.3(1)	85.8(1)	92.1(2)	2.172(4)	2.997(8)	4.292(5)
O(5)	81.6(2)	85.6(2)	161.5(1)	86.6(1)	2.197(4)	3.263(6)
O(6)	102.1(1)	89.8(1)	85.1(2)	173.3(1)	98.0(2)	2.128(4)
			$P(1)P_4$ tetrahedron			
P(1)	O(1)	O(10	O(2)	O(2)		
O(1)	1.533(4)	2.534(8)	2.556(6)	2.490(5)		
O(1)	111.4(3)	1.533(4)	2.490(5)	2.556(6)		
O(2)	111.6(2)	107.4(2)	1.556(4)	2.507(8)		
O(2)	107.4(2)	111.6(2)	107.3(2)	1.556(4)		
			$P(2)O_4$ tetrahedron			
P(2)	O(3)	O(4)	O(5)	O(6)		
O(3)	1.525(4)	2.520(5)	2.510(5)	2.495(6)		
O(4)	107.9(3)	1.590(4)	2.525(6)	2.535(5)		
O(5)	111.0(2)	108.5(2)	1.521(5)	2.510(5)		
O(6)	109.6(2)	108.8(2)	110.9(3)	1.527(4)		
			H atom environment			
O(4)–H		1.06(7)		O(4)–H–O(2)		164(5)
O(2)–H		1.47(7)				
O(4)–O(2)		2.503(5)				
			Na–O distances <3.0 Å			
Na–O(6)		2 × 2.305(3)		O(6)–Na–O(6)		88.7(1)
Na–O(6)		2 × 2.462(5)		O(6)–Na–O(6)		90.0(1)
Na–O(3)		2 × 2.909(6)				
			Mn–Mn distances <3.5 Å			
Mn(2)–Mn(2)		3.179(2)		Mn(2)–O(5)–Mn(2)		93.4(1)
Mn(1)–Mn(2)		2 × 3.369(1)		Mn(1)–O(1)–Mn(2)		98.6(1)
				Mn(1)–O(3)–Mn(2)		100.5(2)

gravimetric analysis shows that $NaMn_3(PO_4)(HPO_4)_2$ undergoes a thermal degradation accompanied by a sudden weight loss at 450°C, corresponding to the loss of one water molecule per formula unit, and apparently transforms to a second phase. The high temperature of transition is consistent with a dehydroxylation process and not a mere dehydration.

The O(4)–H···O(2) bond serves as an additional link between the Mn octahedral chains in adjacent sheets. The straddling of the hydrogen bonds across one tunnel renders what would be the $X(1)$ site inaccessible for cations, but the ensuing distortion creates a new, fairly regular site to accommodate the Na cations. Because the short O(4)–O(2) linkage now constricts the tunnel (0, 1/2, z) across which it straddles, the $P(2)O_4$ tetrahedra tilt outward, simultaneously causing the O(6) atom, bridging Mn(2) and P(2), to jut inward into and pinch the neighboring tunnel (1/2, 1/2, z). Apparently this distortion is sufficient enough to alter the shape of the second tunnel such that the Na atoms no longer reside at the origin, the usual $X(2)$ site in the parent alluaudite structure, but rather at a position translated ±1/4 along z, in a lower symmetry site. Thus, although their covalent frameworks are similar, the structure of $NaMn_3(PO_4)(HPO_4)_2$ is *not* isotypic, strictly speaking, to that of the parent alluaudite, for the cation site is completely different.

The inner coordination environment of the Na atom (at 0, 0.0203, 3/4) is roughly square planar, with fairly regular Na–O bond lengths (2.305(3) and 2.462(5) Å); the two next longest distances at 2.909(6) Å contribute only 0.10 bond valence units to the Na atom. In contrast, the environment of the $X(2)$ site (at 0, 0, 0) in the parent alluaudite is irregular and rhombic, with two very short and two rather long X(2)–O distances (2.080(8) and 2.782(8) Å). The same site (0, 0, 0) in $NaMn_3(PO_4)(HPO_4)_2$ is so distorted, with two extremely short X(2)–O distances (1.689(3) Å), that there is no possibility for a cation to reside here. It is interesting to note that the $X(2)$ site is usually only partially occupied by cations in the natural alluaudites, the more regular $X(1)$ site being occupied preferentially (1, 2). In fact, in the crystal structure determination of the natural alluaudite from Burange (1) and that of a synthetic analogue $NaCdIn_2(PO_4)_3$ (13), the $X(2)$ site is *completely* vacant. On the other hand, in $Cu_{1.35}Fe_3(PO_4)_3$ (14), also a synthetic analogue, some of the Cu atoms enter *not* into the $X(2)$ site at the origin, but rather at a position shifted along z, similar to what happens in $NaMn_3(PO_4)(HPO_4)_2$.

Reactivity. Earlier it was shown that $NaMn_3(PO_4)(HPO_4)_2$ undergoes a decomposition on heating to 450°C, apparently to a second, dehydrated phase of nominal composition $NaMn_3P_3O_{11}$ with a clearly different X-ray powder pattern. This reaction probably entails a condensation of the Mn and P polyhedra. Although it is difficult to predict the structural transformation that is involved, one may surmise that "$NaMn_3P_3O_{11}$" should also be related to the alluaudite structure. Further characterization by X-ray diffraction, electron diffraction, and chemical oxidation experiments are in progress.

In terms of the nomenclature proposed for members of the alluaudite family, the fully reduced end-member composition for the *varulite* subgroup, that is, the series in

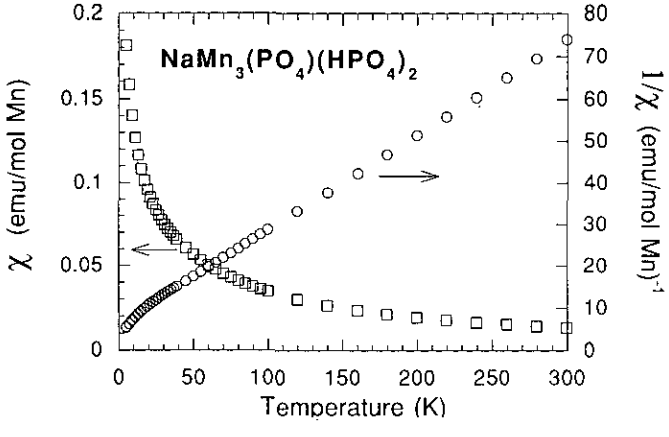

FIG. 3. Plot of magnetic susceptibility and reciprocal susceptibility as a function of temperature or $NaMn_3(PO_4)(HPO_4)_2$.

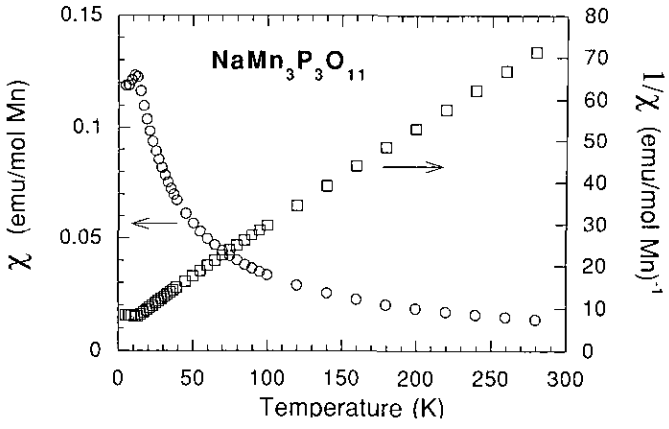

FIG. 4. Plot of magnetic susceptibility and reciprocal susceptibility as a function of temperature for $NaMn_3P_3O_{11}$.

which $M(1) = Mn^{2+}$ and $M(2) = Mn^{2+}$, has been proposed to be $NaCaMn^{2+}(Mn^{2+})_2(PO_4)_3$ and has been predicted to exist (2). Not surprisingly, this end member has never been found naturally, because of the ready substitution of Fe^{3+} for Mn^{2+} in the $M(2)$ site and the concomitant leaching of alkali cations. The compound $NaMn_3(PO_4)(HPO_4)_2$ may be regarded as this end member, if it is formulated as $NaH_2Mn^{2+}(Mn^{2+})_2(PO_4)_3$ with $X(1)$ = two H^+. In view of the large tunnels in which the Na atoms reside in the structure of $NaMn_3(PO_4)(HPO_4)_2$ and the ready oxidation of normal alluaudites, it was thought possible to perform deintercalation. An electrochemical deintercalation was attempted, but this led to the decomposition of the compound. The prevalence of Mn^{2+} in naturally occurring alluaudites has been noted, and indeed, there are no known examples of even a partially oxidized all-Mn form (1, 2). In contrast, an all-Fe synthetic alluaudite, $NaFe^{2+}(Fe^{3+})_2(PO_4)_3$, has been prepared (15). Therefore it remains uncertain whether there is an underlying electronic reason for the absence of a partially oxidized all-Mn form or simply that the right synthetic conditions have yet to be found.

Magnetism. A magnetic study was undertaken in order to confirm the $+\Pi$ oxidation state of Mn, to determine if $NaMn_3(PO_4)(HPO_4)_2$ possesses any interesting low-dimensional magnetic properties arising from the isolated edge-sharing Mn octahedral chains (Fig. 1 and Table 6) and to afford clues to the nature of $NaMn_3P_3O_{11}$.

Figures 3 and 4 show plots of the temperature dependences of the magnetic susceptibility and reciprocal susceptibility for $NaMn_3(PO_4)(HPO_4)_2$ and $NaMn_3P_3O_{11}$, respectively. Both compounds display Curie–Weiss behavior in a wide range of temperatures, having Curie constants of $C = 4.4$ and 4.3 emu K^{-1} per mole Mn for $NaMn_3(PO_4)(HPO_4)_2$ and $NaMn_3P_3O_{11}$, respectively. These values correspond to effective magnetic moments

of $\mu_{eff} = 5.9$ and 5.8 μ_B, respectively, and are consistent with the assignment of high-spin Mn^{2+} (d^5) in octahedral environments (expected spin-only value $\mu_{so} = 5.92\ \mu_B$). The observed Weiss constants are nearly the same for both compounds, $\theta_p \approx -27$ and -26 K, and are negative, implying that the dominant interactions between neighboring Mn atoms are rather weak and antiferromagnetic.

The two compounds behave differently at low temperatures. In $NaMn_3(PO_4)(HPO_4)_2$, no sign of 3D magnetic ordering is detected down to 5K (Fig. 3), although a slight departure from the Curie–Weiss law tending toward higher susceptibilities occurs below ~20 K. This deviation may arise from pretransitional effects associated with the onset of a nonlinear antiferromagnetic ordering occurring below 5 K. In contrast, $NaMn_3P_3O_{11}$ appears to undergo an antiferromagnetic transition at $T_N = 11$ K (Fig. 4). The existence of antiferromagnetic interactions between neighboring Mn^{2+} ions in $NaMn_3(PO_4)(HPO_4)_2$ is consistent with the structural results. Since the MnO_6 octahedra share edges, both direct exchange and Mn^{2+}–O–Mn^{2+} superexchange of the 90° type may be possible. If they occur, the direct interactions should be antiferromagnetic, whereas the net d^5–d^5 90° exchange is expected to give antiparallel coupling because of the relatively large contribution from e_g–p_y–d_{yz}, e_g–p_z–d_{yz}, and d_{xy}–p_x–d_{xy} paths (16). However, it would appear that these antiferromagnetic intrachain couplings are not strong enough relative to the interchain interactions as we do not observe 1D antiferromagnetic properties.

CONCLUSION

The compound $NaMn_3(PO_4)(HPO_4)_2$ may be considered to be an unoxidized variant and thus a long-sought end member of the alluaudite structure type, but it involves hydrogen bonding in its framemwork and a distinctly different cation site. Unlike known, naturally occurring alluaudites, $NaMn_3(PO_4)(HPO_4)_2$ has been prepared under reducing conditions. Although it is not easily oxidized, it appears to undergo a dehydroxylation at 450°C to transform to a second phase with nominal composition $NaMn_3P_3O_{11}$.

ACKNOWLEDGMENT

A.M. thanks NSERC Canada for financial support in the form of a postdoctoral fellowship.

REFERENCES

1. P. B. Moore, *Am. Mineral.* **56,** 1955 (1971).
2. P. B. Moore and J. Ito, *Mineral. Mag.* **43,** 227 (1979).
3. M. Tsuji, S. Komarneni, Y. Tamaura, and M. Abe, *Mater. Res. Bull.* **27,** 741 (1992).
4. K. Yvon, W. Jeitschko, and E. Parthé, *J. Appl. Crystallogr.* **10,** 73 (1977).
5. G. M. Sheldrick, "SHELXTL PLUS 4.0." Siemens Analytical X-Ray Instruments, Inc., Madison, WI, 1990.
6. D. T. Cromer and J. T. Waber, *in* "International Tables for X-Ray Crystallograph," Vol. IV, Tables 2.2B and 2.3.1. Kynoch, Birmingham, England, 1974.
7. N. E. Brese and M. O'Keeffe, *Acta Crystallogr. Sect. B* **47,** 192 (1991).
8. I. D. Brown and D. Altermatt, *Acta Crystallogr. Sect. B* **41,** 244 (1985).
9. J. Moring and E. Kostiner, *J. Solid State Chem.* **61,** 379 (1986).
10. P. Lightfoot, A. K. Cheetham, and A. W. Sleight, *J. Solid State Chem.* **73,** 325 (1988).
11. R. D. Shannon, *Acta Crystallogr. Sect. A* **32,** 751 (1976).
12. W. C. Hamilton and J. A. Ibers, "Hydrogen Bonding in Solids," Benjamin, New York, 1968.
13. D. Antenucci, G. Miehe, P. Tarte, W. W. Schmahl, and A.-M. Franslot, *Eur. J. Mineral.* **5,** 207 (1993).
14. T. E. Warner, W. Milius, and J. Maier, *J. Solid State Chem.* **106,** 301 (1993).
15. D. R. Corbin, J. F. Whitney, W. C. Fultz, G. D. Stucky, M. M. Eddy, and A. K. Cheetham, *Inorg. Chem.* **25,** 2279 (1986).
16. J. B. Goodenough, "Magnetism and the Chemical Bond." Wiley–Interscience, New York, 1969.